Establishment of a multi-purpose 3D geodetic reference frame for deformation monitoring in Cortes de Pallas (Spain)

Luis García-Asenjo[1], Laura Martínez[2], Sergio Baselga[1], Pascual Garrigues[1]

[1] Department of Cartographic Engineering, Geodesy and Photogrammetry, Universitat Politècnica de València, Camino de Vera s/n, 46022 Valencia, Spain, (lugarcia@cgf.upv.es)
[2] Department of Roads and Infrastructures, Diputació de València, c/ Hugo de Moncada, 9, 46010 Valencia,Spain, (laura.martinez@dival.es)

ABSTRACT

La Muela, which is a cliff near Cortes de Pallás in Valencia (Spain), partially collapsed in 2015. After the refurbishment and consolidation works the Universitat Politècnica de València was commissioned by the Diputació de València to undertake a three-year deformation monitoring project based on discrete geodetic surveys by using high-precision distance meter techniques. This solution was planned to establish a 3D high-precision reference frame, to monitor the possible deformation of 15 target points of interest on the cliff, and to provide precise ground control to image-based techniques or other techniques that might be used in the future. The measurements were carried out using a Kern ME5000 Mekometer, a 3D network of data loggers for temperature, humidity and air pressure, and the submillimetric GNSS-Based Distance Meter approach as developed by the UPV. The absolute scale of the network is guaranteed by the calibration of the instruments at the UPV calibration baseline, which is metrologically traced to the SI-metre, as well as laboratory calibration of meteorological sensors. This contribution describes the methodology and processes that were applied to determine the coordinates of the first geodetic campaign which was carried out in June 2018. The results show that the 3D coordinates were obtained with an accuracy of some tenths of a millimeter for the reference frame pillars and one millimeter for the target points. The comparison with other techniques confirms the importance of using metrologically sound reference frames as a crucial tool for a proper integration of different deformation monitoring techniques.

I. INTRODUCTION

Cortes de Pallás is a Cretaceous limestone area with historical geotechnical problems (Alonso *et al*. 1993). In 6th April 2015, a cliff called La Muela partially collapsed, and some facilities of the electricity power plant and the main access road to the village were seriously damaged. The consolidation works, commissioned by the Road and Infrastructures Department of the Diputació de València, involved a variety of solutions to cope with large landslides such as sanitation of rocky volumes, both static and dynamic barriers, anchoring and bolts or triple metal torsion meshes (see Fig. 1).
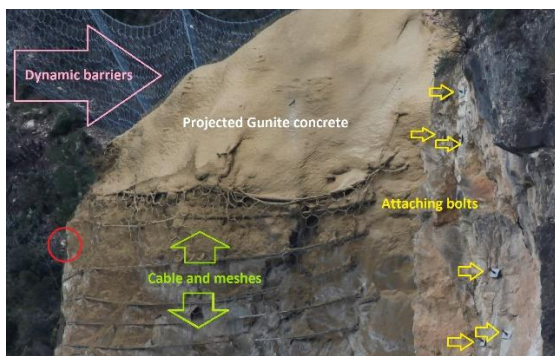
Figure 1. Barriers (pink), cables and meshes (green), anchoring bolts (yellow), and one target point (red)

As known from experience, it is highly advisable to supplement those systems with a deformation monitoring plan to detect possible displacements of huge boulders or potential dysfunction of the installed anchoring systems.

However, to detect displacements of some centimetres with the required level of significance, the position of the target points of interest should be determined with a precision of at least some millimeters, which is a quite challenging task due to the peculiar orography of the zone. Being La Muela an almost vertical cliff facing a water reservoir, the measurements have to be necessarily done from the opposite shoreline which is some 600 m apart. To give a clearer picture of the limitations, the whole area involves distances from 500 to 2000 m with height differences reaching 500 m, and the target points are only accessible by professional climbers using abseiling techniques.

Among the currently available solutions for deformation monitoring one can find SAR techniques, monitoring systems based on total stations (TS), image-based methods, or high-precision distance meter techniques (EDM). Since La Muela is vertical and faces North, InSAR (Colesanti *et al*., 2003) or GBSAR techniques (Montserrat *et al*., 2014) cannot be efficiently applied. Moreover, the behavior of large

limestone blocks, which is the case at hand, is different from landslides where those techniques have proved successful (Del Ventisette *et al.*, 2011). Monitoring solutions based on permanent total stations can achieve a good repeatability (VIM, 2012). Nonetheless, air refraction greatly diminishes their efficiency in terms of reproducibility and accuracy (VIM, 2012), and they can only be used for a discrete number of the target points. On the contrary, methods based on image sensors such as terrestrial laser scanning (TLS) or photogrammetry, can massively collect information, although they require a precise ground control and are similarly affected by refraction.

After careful consideration, the Diputació de Valencia opted for periodical geodetic surveys (Niemeier, 1981; Caspary, 1987) by using high-precision distance meter techniques (EDM) with a triple objective: to establish a high-precision 3D reference frame, to determine the 3D coordinates of 15 target points placed in specific point of interest, and to provide ground control to image-base techniques. An additional reason to set up a high-precision 3D geodetic reference frame is to facilitate the proper integration of current solutions with new solutions or technologies that could be applied in the future. Nonetheless, to serve this purpose, the reference frame needs to be precise, but also accurate in a metrological sense so that the scale is consistent with the unit of length of the International System (SI).

II. Geodetic network and target points

Pillars and reflectors (RFLs) were set up in 2017. After the required settling time, the first field campaign using submillimetric EDM techniques was carried out in July 2018.

The reference frame is a geodetic network with ten pillars which surround the 15 target points (see Fig.2).
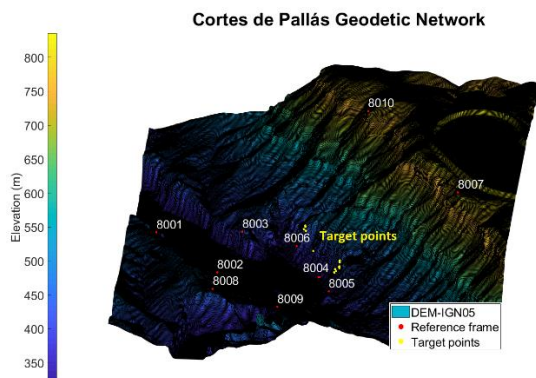
Figure 2. Reference frame and target points

The target points are measured from pillars 8001, 8002, 8003, 8004, 8005, 8008, and 8009, while pillars 8006, 8007 and 8010 strengthen the geometry of the network so as to accomplish the required 3D sub-millimetric precision for the reference frame. Pillar 8007 is also a point of the Fourth Order Network of the Valencian Cartographic Institute (ICV).

With regard to the target points, Fig. 2 illustrates how they have been located in groups either to detect displacements of specific limestone boulders (Fig. 3) or to detect dysfunctional behavior of the attaching systems (Fig. 2).
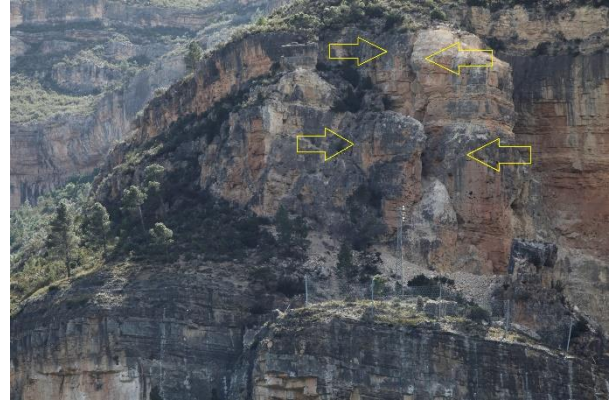
Figure 3. Example of a group of four target points. For the sake of size comparison please note the size of the medium voltage electrical tower

Each target point consists of one Leica 360 reflector and one standard target sphere (Ø145 mm) which are rigidly mount and firmly attached to the rock (Fig. 4). Since the installation process had to be done under non-favorable conditions by abseiling, their verticality cannot be taken for granted and the determination of the attitude becomes crucial to transfer coordinates between the center for distances and the center for images.
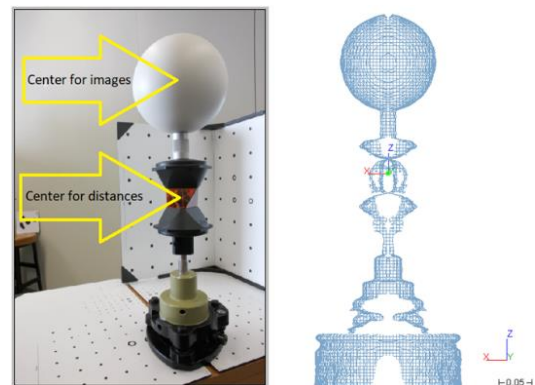
Figure 4. The set installed in the target point, which consisted in a set formed by one Leica 360RFL and an white sphere, was measured in laboratory by using a combination of photogrammetry and TLS techniques.

III. Measurement process

The first measurement campaign was carried out from 16 to 19 July 2018. Prior to measurements each pillar was equipped with a data-logger Testo 176P1 and a parasol.

All the distances (~ 250) were measured using the Kern ME5000 Mekometer SN 357050. For distances between pillars (~ 100) four original Kern RMO5035

RFLs were used, while for target points, distances were measured to Leica 360 reflectors (~ 150).

The measurement of each distance takes approximately two minutes while the observer measures the meteorological parameters using a traditional Thies Clima Assmann-Type psychrometer (± 0.2 K) and a Thommen 3B4.01.1 aneroid barometer (± 0.3 hPa) and the digital meteorological station is automatically recording values.

All the meteorological sensors were previously calibrated at the UPV calibration laboratory. The results for the Testo 176P1 data-loggers showed that their accuracy under laboratory conditions was ± 0.2 K and ± 1.8 hPa for temperature and air pressure respectively. Nonetheless, we were aware that some differences between the traditional and the digital sensors could be found under real field conditions.

Figure 5. Pillar equipped with a parasol and a data-logger for dry and wet temperatures as well as air pressure.

Therefore, air temperature, humidity and pressure were always double-checked at the EDM end (Fig. 6).

Figure 6. Distance measurement with the ME5000 Mekometer. Both traditional and digital meteorological sensors were simultaneously used at the EDM end.

Therefore, a comparison between the two types of meteorological parameters was done, and we found significant differences for both dry and wet temperatures that were corrected by using the following correction functions

$$T_d^c = T_d^m + a_d T_d^m + a_w T_w^m + a_p P^m \qquad (1)$$
$$T_w^c = T_w^m + b_d T_d^m + b_w T_w^m + b_p P^m$$

where

T_d^m, T_d^c = Measured and corrected dry temperature
T_w^m, T_w^c = Measured and corrected wet temperature
P^m = Measured air pressure

with coefficients

$a_d =$	0.213 ± 0.039	$b_d =$	0.109 ± 0.024
$a_w =$	0.061 ± 0.008	$b_w =$	-0.051 ± 0.005
$a_p =$	-0.009 ± 0.001	$b_p =$	0.002 ± 0.001

IV. LENGTH METROLOGY

A. Calibration of the reflectors

All the reflectors were calibrated at the UPV calibration baseline (Garcia-Asenjo et al., 2016) in accordance with the full procedure of ISO 17123-4 (2012). The results obtained for the four original Kern RMO5035 that were used to measure the reference frame are shown in Table 1. The results obtained for the fifteen Leica 360 RFLs located in the target points ranged from 24.41 mm to 24.88 mm with standard deviations from 0.06 mm to 0.09 mm.

Table 1. Results of the calibration process for the used Kern RMO5035 RFLs.

Reflectors S/N	Offsets	
	Value	Sigma
374447 (UCM)	0.0868	0.0183
374448 (UCM)	0.1224	0.0133
365628 (UPV)	0.0791	0.0584
358811 (UPV)	0.0979	0.0852

However, being the RFLs omnidirectional, the offset depends on the angle of incidence. For that reason, RFLs No 1 and No 15 were additionally calibrated by rotating them every 5 degrees. Interestingly, the measured values were consistent with the theoretical model as described in its white paper (Fig. 7).
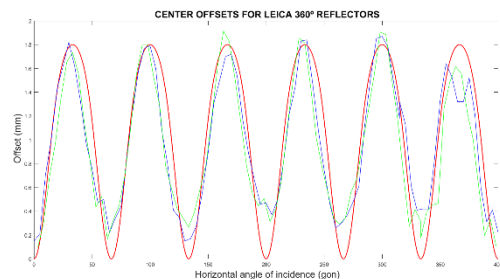
Figure 7. Centre offsets measured for reflectors 01 (blue) and 15 (green). The red line shows the theoretical model.

Therefore, the nominal offset error provided by the manufacturer (2 and 3 mm for horizontal and vertical components respectively) could be potentially reduced up to some tenths of a millimeter as long as the

attitude of each reflector is known. Nevertheless, this correction has not been applied in the first campaign because we have seen that the residual refraction for distances measured to target points is of the same order.

B. *Stability of the EDM frequency and scale*

According to the initial calibration in 1989, the ME5000 Mekometer (SN 357050) was adjusted to have a nominal carrier frequency of 479.35817 MHz with a scale factor of 0.99999994. Due to the quartz oscillator ageing, this scale factor changes with time. For this reason, the frequency was measured in the UPV calibration laboratory just after the measurement campaign. The measured frequency was 480.03060 MHz which results in a scale factor of 1.000000980. This scale factor can only be checked by using a calibration baseline where the nominal distances are known with a better accuracy than the distances provided by the EDM at hand. Since distances in Cortes de Pallás range from 200 to 2000 m and the Mekometer yields sub-millimetric precision, the optimal metrological facility should have a length of 5 km with distances known within 1 mm of uncertainty. At present such type of facility is not available; however, the European Research Project 18SIB01 Large-scale dimensional measurements for geodesy (GeoMetre) is expected to provide one as metrologic standard for the surveying community by year 2022.

V. Computing process

Prior to the adjustment the following corrections were applied: refraction correction, EDM frequency drift correction and geometric correction. Once these corrections were applied and their corresponding errors computed in order to contribute to the stochastic model, the resulting slope distances were 3D adjusted in an Earth Centered Earth Fixed (ECEF) coordinate system in two steps. In the first step, only distances between pillars were adjusted to provide a solution for the frame. In the second step, only distances to target points were adjusted with the pillar coordinates kept fixed. Finally, as requested by the Road and Infrastructures Department of the Diputació de València, all the resulting coordinates and precisions were converted into geodetic coordinates with ellipsoidal height (φ,λ,h), TM30 with orthometric height (E,N,H), and the local system CP2017 (x,y,z).

Following, some important aspects are furtherly explained.

A. *Approximate coordinates*

Since only distance measurements have been included in the computing process and they are expected with sub-millimetric precision, the initial coordinates for the adjustment are required to be known with a precision better than one centimeter. In addition, for geomatic management purposes, the

Road and Infrastructures Department of the Diputació de València usually demands all commissioned works to be delivered in the official geodetic reference system (ETR89) as realized by the Spanish official frame (REGENTE/REDNAP), which in turn is densified by the Valencian Fourth Order Network. Therefore, a previous geodetic survey using both GNSS receivers and a Leica TM30 total stations was carried out to obtain an initial set of coordinates that were consistent with the official ETRF89 frame within 1 cm, with the official ETRS89 coordinates of pillar 8007 kept fixed for all the subsequent computations. Then, using only the distances measured with the ME5000 Mekometer, the coordinates obtained after two iterations were retained as approximate coordinates for the final adjustment. This approximate solution, which was called CPFRAME_00, is consistent with the ETRS89 system as locally realized and its precision is the order of some millimeters.

B. *Refraction correction*

For each distance, both the air index n and coefficient K of refraction were determined at both ends by means of the meteorological parameters. The index of refraction n was computed using the expression for the refraction index recommended in the resolution from the General Assembly of the IUGG when the required precision is 10^{-7} (International Union of Geodesy and Geophysics, 1999; Ciddor, 1996; Ciddor and Reginald, 1999; Ciddor 2002) and the coefficient of refraction K was obtained from the usual expression (Dodson and Zaher, 1985; Baselga *et al.*, 2014).

Once the values of n and K are determined at both ends, the average value is used to compute the first and second velocity corrections as well as the arch-to-chord correction (Bell, 1992; Rüeger, 1996). As expected, the last two corrections were negligible, but the values obtained for the first velocity correction ranged from 5.81 mm to 64.74 mm.

Subsequent residual analysis showed that the applied refraction correction proved accurate for those distances that meteorological parameters could be measured at both ends (pillars), while the applied correction worked worst for target points, where the meteorological data was obtained by interpolation. For all the 98 reference frame distances, only 11 have residuals with and absolute value above 1 mm, and only one (2.71 mm) was detected as an outlier. On the contrary, for the 162 target point distances, residuals ranged from -2.88 mm to 3.56 mm, which is one order of magnitude more if compared to the reference frame ones.

Taking into account that errors for Leica 360 RFLs are below 3 mm, the bulk of residuals for target points can be largely explained by the mismodelled refraction.

C. *EDM frequency correction*

As previously mentioned, the nominal EDM carrier frequency of 479.35817 MHz experiences a slow over time drift due to the quartz oscillator ageing. The actual frequency of the ME5000 Mekometer SN 357050 was measured by the UPV calibration laboratory in 15 July 2015, 17 November 2016, and 20 July 2018 and the resulting frequencies were 479.35776 MHz, 479.5773 MHz and 479.35770 MHz respectively, which in turn give the scale factors 1.000000855, 1.000000918, and 1.000000980. Since all of the measured distances were certified with an uncertainty of ± 0.01 kHz, the influence on the resulting scale is of the order 10^{-10} and thus negligible. The application of the scale factor gives always a positive proportional correction which ranges from 0.21 mm to 1.72 mm.

As explained before, this scale cannot be externally assessed due to the lack of calibration baselines for distances of several km whose nominal distances are known with 10^{-7} uncertainty. At present, only Nummela Standard Baseline in Finland (Jokela *et al.*, 2010) can provide that level of uncertainty, but its maximum length is limited to 864 m. Moreover, transferring absolute scale from Nummela to this geodetic network would entail two extra weeks of measurements in Finland, which is expensive and time consuming.

A possible and more feasible alternative is the use of GNSS techniques as distance meter. Previous research conducted by the authors have shown that, for short and fairly horizontal distances, GNSS techniques can provide absolute distances with submillimetric accuracy (Baselga *et al.*, 2013; Baselga *et al.*, 2014b; Baselga *et al.*, 2015; García-Asenjo *et al.*, 2017). So, we considered that measuring the baseline 8007-8010 using our GNSS-Based Distance Meter approach (GBDM) would be interesting for two reasons. Firstly, we could collect GNSS data to improve our GBDM which is still under development, and secondly, we would be able to externally assess the scale of the geodetic network as provided by the ME5000 Mekometer.

D. *Geometric reductions*

The measured distance is referred to the center of the EDM and the corresponding RFL. Since the height above pillars of EDM and RFL are different and vary from one station to other, distances have to be geometrically corrected in order to obtain the distances between the head of pillars. This geometrical correction requires the heights to be accurately measured (better than 1 mm) and good approximate coordinates. In addition, it can be computed either using local coordinates and simplified expressions or using geodetic coordinates and a rigorous method.

Table 2. Example of the differences found between the rigorous and the approximate geometrical correction. All values are expressed in mm.

Distance	Rigorous		Approximate	
	Value	Error	Value	Error
8009-8010	0.25	0.18	0.32	0.16
8009-8007	-2.06	0.37	-2.00	0.20
8009-8003	-0.17	0.13	-0.14	0.07
8009-8001	93.28	0.36	93.06	0.10
8009-1001	89.56	0.93	89.35	0.42
8009-1002	-0.21	0.92	-0.20	0.41
…	…	…	…	…

No matter the method, the measuring errors of the heights as well as the errors of the approximate coordinates have to be properly propagated in order to contribute to the stochastic model.

As an illustration, Table 2. shows the value of the correction and their corresponding propagated error for several distances that is obtained by used both methods. As can be seen, the value of the correction differs some tenths of a millimeter, but there is a significative difference between the propagated errors. The approximated method seems to be too optimistic, especially for distances measured to target points, where the height is considered null, but its error is assumed to be 2 mm in concordance with the Leica 360 technical specifications. Consequently, we opted for the rigorous method.

E. *Functional model*

The corrected slope distances were adjusted using the following functional model

$$-\frac{X_j - X_i}{D_{ij}^c} dX_i - \frac{Y_j - Y_i}{D_{ij}^c} dY_i - \frac{Z_j - Z_i}{D_{ij}^c} dZ_i + \frac{X_j - X_i}{D_{ij}^c} dX_j +$$

$$\frac{Y_j - Y_i}{D_{ij}^c} dY_j + \frac{Z_j - Z_i}{D_{ij}^c} dZ_j - (D_{ij}^c - D_{ij}^m) = v_{ij} \qquad (2)$$

where

$D_{ij}^c = \sqrt{(X_j - X_i)^2 + (Y_j - Y_i)^2 + (Z_j - Z_i)^2}$
is the computed distance from i to j
D_{ij}^m is the measured and subsequently corrected distance from i to j
(X_i, Y_i, Z_i) are the ECEF coordinates of i
(X_j, Y_j, Z_j) are the ECEF coordinates of j

As mentioned, the resulting ECEF coordinates and their precisions were subsequently converted into different useful horizontal and vertical coordinate systems: geodetic, TM30, and both ellipsoidal and orthometric heights. Additionally, a conventional cartesian system called CP2017 was locally defined to facilitate the future deformation analysis as well as the processing and integration of image-based techniques.

Table 3. Conventional definition of the CP2017 local system.

Parameter	Value
$x_0 =$	800.0000 m
$y_0 =$	800.0000 m
$z_0 =$	150.0000 m
$\varphi_0 =$	39°14'47.98063''
$\lambda_0 =$	-0°55'55.55670''
$h_0 =$	520.57344 m
$\alpha_0 =$	230.0000 gon

The azimuthal rotation α_0 situates the xz-plane of the local system fairly coincident with the cliff of interest.

VI. RESULTS

A. Reference frame solution

The weighs were computed according to a rigorous stochastic model which included the propagation of all possible sources of error. On average, the a priori error considered for distances was approximately 0.5 mm.

The variance of unit weight was 1.221, with 77 degrees of freedom, and $\hat{\chi}^2 = 94.018$. Since $\chi^2_{(0.05,77)} = 42.576 < \hat{\chi}^2 < \chi^2_{(9.95,77)} = 124.475$, H_0 is accepted. Respectively, Table.4 and Table.5 show the adjusted coordinates and their corresponding precision.

Table .4 Local coordinates of the reference frame pillars

	Local coordinates (CP2017)		
Site	x (m)	y(m)	z (m)
8001	159.4083	94.2080	144.9715
8002	536.2871	341.2314	46.7024
8003	285.0310	608.8918	106.5783
8004	776.2580	914.5217	14.9182
8005	1077.0223	854.3889	74.0872
8007	1224.7750	1647.0658	499.7153
8008	929.5876	147.6371	155.1183
8009	981.7671	554.0390	10.4536
80010	53.8649	1536.3211	467.0790

Table 5. Standard deviation of the reference frame pillars

Site	Error		
	σ_x (mm)	σ_y (mm)	σ_z (mm)
8001	0.7	0.7	0.6
8002	0.4	0.4	0.5
8003	0.3	0.4	0.5
8004	0.7	0.7	1.2
8005	0.8	0.5	0.8
8007	0.1	0.1	0.1
8008	0.4	0.6	0.7
8009	0.6	0.7	0.7
8010	1.1	1.1	1.2

The analysis of residuals showed that 85.7% of them were below 1 mm, and only one of the distances measured between pillars 8001 and 8010 was detected as an outlier by both Baarda and τ tests.

B. Target points solution

The weighs were computed according to a rigorous stochastic model which included the propagation of all possible sources of error. In this case, the a priori error considered for distances was approximately 5 mm.

The variance of unit weight was 1.269, with 114 degrees of freedom, and $\hat{\chi}^2 = 144.705$. Since $\chi^2_{(0.05,77)} = 70.754 < \hat{\chi}^2 < \chi^2_{(9.95,77)} = 170.314$, H_0 is accepted. Respectively, Table.6 and Table.7 show the adjusted coordinates and their corresponding precision.

Table 6. Local coordinates of the target points

	Local coordinates (CP2017)		
Site	x (m)	y(m)	z (m)
1001	912.8108	1005.2084	144.7208
1002	908.1700	1007.6356	139.8012
1003	901.4871	1010.6389	145.7455
1004	922.0150	999.5838	118.6362
1005	917.9428	999.3877	114.3216
1006	926.8292	996.9338	111.7634
1007	894.6261	988.8788	86.0142
1008	874.9508	983.5045	71.6587
1009	873.2529	991.7038	85.6273
1010	619.6238	950.3059	85.5166
1011	495.6261	952.8132	138.6876
1012	480.6799	954.6206	158.9148
1013	479.1463	946.6025	141.6632
1014	488.0169	952.9289	156.1855
1015	900.0689	983.5999	80.8598

Table 7. Standard deviation of the target points

Site	Error		
	σ_x (mm)	σ_y (mm)	σ_z (mm)
1001	0.9	0.6	0.9
1002	1.0	0.7	1.5
1003	1.0	0.7	1.5
1004	1.3	0.8	1.6
1005	0.9	0.6	1.5
1006	0.9	0.6	1.5
1007	0.9	0.6	1.6
1008	0.3	0.4	1.6
1009	0.4	0.4	1.5
1010	0.4	0.4	1.3
1011	0.6	0.5	1.1
1012	0.7	0.6	1.1
1013	0.6	0.5	1.1
1014	0.6	0.5	1.0
1015	0.7	0.7	1.5

The analysis of residuals showed that 74.8% of them were below 1 mm, and only the distance measured between pillar 8009 and reflector 1001 was detected as an outlier by both Baarda and ⊠ tests.

C. *Comparison with GNSS*

The baseline 8007-8010 was selected to test our GBDM approach for two reasons. First, since there is no direct line of sigh between those pillars, the GNSS-derived distance could be used to strength the EDM solution. Second, being the baseline longer than 1 km with some 30 m of height different, the measurements can be used to test and improve our GBDM approach in the context of the objective number three of the GeoMetre project, which aims at developing technologies and methods capable to provide distances of at least 5 km with uncertainties of 1 mm order.

Figure 8. Leica AR25.R3 choke-ring antenna set up at dusk for GNSS distance measurement between pillars 8007 and 8010, which do not have straight sight between them.

The GNSS measurements were carried out using two Trimble 5700 GPS receivers along with two individually calibrated Leica AR25.R3 choke-ring antennas. GPS data were collected in twelve-hour sessions overnight, and processed using the UPV GBDM approach (Baselga *et al.*, 2015; García-Asenjo *et al.*, 2017) along with IGS final orbits.

Following, a summary of the results is provided along with the comparison with the distanced obtained derived from the adjusted coordinates of the reference frame solution.

Table 8. Adjusted coordinates obtained by using the UPV GBDM approach

	ECEF coordinates (ITRF2014, epoch 2018.6299088)	
	8007	8010
X (m)	4946667.0442	4946259.2700
Y (m)	-80473.8729	-79474.0856
Z (m)	4013378.3069	4013845.7516

Therefore, the GBDM distance = 1176.58787 m ± 0.10 mm can be compared to the distance derived from the reference frame solution distance = 1176.58830 m ± 1.31 mm. Thus, the difference is -0.432 mm. The standard deviations for both GBDM and network solutions have been properly propagated from the corresponding covariance matrices.

VII. CONCLUSIONS AND FUTURE WORK

There is an increasing demand of techniques and methods to perform accurate deformation monitoring in order to mitigate geotechnical risks, as it is the case of Cortes de Pallás. Currently available techniques for deformation monitoring such as SAR, GNSS, total stations, photogrammetry, terrestrial laser scanning, or mobile mapping contribute to the development of integral geomatic solutions and can facilitate an efficient management of those risky situations. Nonetheless, when the case at hand requires accuracies at 1 mm level at 1-2 km, and the zone has strong limiting conditions, which is the case in Cortes de Pallás, proper integration requires the use of the most advanced geodetic techniques.

The results obtained in the first campaign carried out in Cortes de Pallás demonstrate that accurate millimetric solutions can be obtained even when distances are longer than 1 km by using long-range submillimetric EDM techniques along with length metrology concepts and methods. Additionally, the UPV GBDM approach has shown promising results even when the measured distance is over 1 km and slightly sloped. Nevertheless, to come to definitive conclusions valid for length metrology, there is still a long way to go.

Unfortunately, long-range submillimetric EDM techniques are no longer commercially available and only a few ME5000 Mekometer, which were manufactured in the late 80s, are still working. Therefore, there is a real need to develop new techniques, methods, and outdoor metrologic facilities to provide accurate distances (1 mm uncertainty) in the range of 10 to 5000 m. All the potential solution to this challenging problem, for instance GBDM techniques, have to prove metrologically sound in research projects like the EURAMET-EMPIR-18SIB01 GeoMetre that has been recently fund.

VIII. ACKNOWLEDGEMENTS

References

Alonso, E.E., Gem, A., and Lloret, A. (1993). Géotechnique 43, No. 4, 507-521

Baselga, S., García-Asenjo, L., and Garrigues, P. (2013). Submillimetric GPS distance measurement over short baselines: case study in inner consistency. *Meas. Sci. Technol*. (24) 075001.

Baselga, S., García-Asenjo L., and Garrigues P. (2014a). Practical Formulas for the Refraction Coefficient. *J. Surv. Eng.* 140(2): 06014001

Baselga S., García-Asenjo L., and Garrigues P. (2014b). Submillimetric GPS distance measurement over short baselines: noise mitigation by global robust estimation. *Meas. Sci. Technol*. (25)105004.

Baselga, S.,García-Asenjo, L. andGarrigues, P. (2015) Submillimetric GNSS distance determination for metrological purposes. In Proc. 5th International Colloquium Scientific and Fundamental Aspects of the Galileo Programme. (27 - 29 October 2015, Braunschweig, Germany).

Bell B. (1992). Workshop on the Use and Calibration of the Kern ME5000 Mekometer. *Proc. Stanford Linear Accelerator Center*, Stanford University, USA,18-19 June, p 1-80.

Caspary, W. F. (1987) Concepts of network and deformation analysis (School of Surveying, The University of New South Wales, Australia), Monograph 11.

Ciddor, P.E. (1996). Refractive index of air: new equations for the visible and near infrared. *Appl. Opt.* 35, 1566 - 1573

Ciddor, P.E., and Reginald J.H. (1999). Refractive index of air. 2. Group index. . *Appl. Opt.* 38, 1663 – 1667

Ciddor, P.E. (2002). Refractive index of air: 3. The roles of CO_2, H_2O, and refractivity virials. *Appl. Opt.* 41, 2292 – 2298

Colesanti, C., Ferretti, A., Prati, C., and Rocca, F. (2003). Monitoring landslides and tectonic motions with the Permanent Scatterers Technique. *Engineering Geology* 68 (2003) 3 –14

Del Ventisette, C., Intrieri, E., Luzi, G., Casagli, N., Fanti, R. , and Leva, D. (2011). Using ground based radar interferometry during emergency: the case of the A3 motorway (Calabria Region, Italy) threatened by a landslide. Nat. Hazards Earth Syst. Sci., 11, 2483–2495, 2011.

Dodson, A. H., and Zaher, M. (1985). Refraction effects on vertical angle measurements. *Surv. Rev.*, 28(217), 169–183.

García-Asenjo, L., Baselga, S., and Garrigues, P (2016). Deformation Monitoring of the Submillimetric UPV Calibration Baseline. *Journal of Applied Geodesy*, 11(2), pp. 107–114.

García-Asenjo, L., Atkins, C., Baselga, S., Ziebart, M., Garrigues, P., and Luján, R. (2017). Submillimetric GNSS Distance Determination with Multipath Mitigation. Proc. 6th International Colloquium on Scientific and Fundamental Aspects of GNSS / Galileo. (25 - 27 October 2017). Valencia, Spain.

International Union of Geodesy and Geophysics (IUGG). (1999). "Resolutions adopted at the XXII General Assembly by the IUGG Associations." Proc., Univ. of Birmingham, Birmingham, U.K., 110–111.

ISO 17123-4 (2012). Optics and optical instruments. Field procedures for testing geodetic and surveying instruments. Part 4: Electro-optical distance meters (EDM instruments).

Jokela, J. and Häkli, P. (2010). Interference Measurements of the Nummela Standard Baseline in 2005 and 2007. Publications of the Finnish Geodetic Institute. No. 144.

Monserrat, O, Crosetto,M., and Luzi, G. (2014). A review of ground-based SAR interferometry for deformation Measurement. ISPRS *Journal of Photogrammetry and Remote Sensing* 93 (2014) 40–48.

Niemeier, W. (1981) Statistical tests for detecting movements in repeatedly measured geodetic networks. Tectonophysics 71, 335–351.

Rüeger, J. M. (1996) Electronic Distance Measurement (Springer).

VIM (2012). International vocabulary of metrology. Basic and general concepts and associated terms. *Joint Committee for Guides in Metrology*.